Available online at www.sciencedirect.com

ScienceDirect

Journal of Magnesium and Alloys 2 (2014) 1–7
www.elsevier.com/journals/journal-of-magnesium-and-alloys/2213-9567

Full length article

# Role of multi-microalloying by rare earth elements in ductilization of magnesium alloys

Yuanding Huang*, Weimin Gan, Karl Ulrich Kainer, Norbert Hort

*Institute of Materials Research, Helmhlotz-Zentrum Geesthacht, Max-Planck-Str. 1, D-21502 Geesthacht, Germany*

Received 5 November 2013; accepted 2 January 2014
Available online 13 March 2014

**Abstract**

The present work investigates the influences of microalloying with rare earths on the mechanical properties of magnesium alloys. The amount of each rare earth element is controlled below 0.4 wt.% in order not to increase the cost of alloy largely. The synergic effects from the multi-microalloying with rare earths on the mechanical properties are explored. The obtained results show that the as-cast magnesium alloys multi-microalloying with rare earths possesses a quite high ductility with a tensile strain up to 25–30% at room temperature. Moreover, these alloys exhibit much better corrosion resistance than AZ31 alloy. The preliminary *in situ* neutron diffractions on the deformation of these alloys indicate that the multi-microalloying with rare earths seems to be beneficial for the activation of more slip systems. The deformation becomes more homogeneous and the resultant textures after deformation are weakened.


*Keywords:* Microalloying; Magnesium alloy; Ductility; Rare earth element

## 1. Introduction

Mg alloys with a low density and high specific strength is an ideal structure engineering materials for light-weighting applications. Compared with the traditional steel or aluminum materials, they have not been widely accepted by consumer. Their commercial products are mainly fabricated by die casting. In contrast to cast products, the wrought Mg alloys only have a small market with a proportion of less than 5% [1]. The main obstacles to prevent the wrought products from widespread applications are their low ductility/toughness and poor corrosion [2]. Therefore, to improve the formability and corrosion resistance becomes an urgent issue to extend the applications of Mg alloys.

The low ductility/toughness of magnesium is due to the intrinsically brittle nature of the hexagonal close-packed (h.c.p) crystal structure. The critical resolved shear stress of the basal <a> slip system of single-crystal Mg is approximately 1/100 of that of other slip systems at room temperature [3,4]. The basal <a> slip occurs readily in comparison with the other slip systems. Consequently, the formation of sharp basal <a> or near basal deformation textures leads to a high deformation anisotropy in Mg.

For magnesium alloys, three main reasons are responsible for their poor corrosion resistance. First, they are highly susceptible to galvanic corrosion, usually observed as heavily localized corrosion in the regions adjacent to the cathode. The cathodes can be external as other metals in contact with magnesium, or may be internal as second phases or impurity phases [5]. Second, the quasi-passive hydroxide film on the surface is

* Corresponding author. Tel.: +49 4152871935; fax: +49 4152871909.
*E-mail addresses:* yuanding_huang@hotmail.com, yuanding.huang@hzg.de (Y. Huang).
Peer review under responsibility of National Engineering Research Center for Magnesium Alloys of China, Chongqing University

Production and hosting by Elsevier

http://dx.doi.org/10.1016/j.jma.2014.01.005.

not as stable as the passive films formed on aluminum [6]. Finally, as the components used in the automotive, the stress corrosion cracking is also one of dangerous reasons accounting for the limit of applications [7].

In order to overcome the above-mentioned problems encountered in Mg alloys, the multi-micro-alloying concept is introduced to develop new wrought Mg alloys [8,9]. The used alloying elements are mainly those rare earth elements with a large solubility in Mg. The designed alloys are close to a single phase solid solution. They were nominally expressed as Mg−REs−0.5Zr (wt.%). REs stands for rare earths elements; zirconium (Zr) was mainly used as the grain refiner [10]. Recent results demonstrated that the addition of REs is the most promising method to weaken the texture and improve the deformability of magnesium alloys [11−14]. Agnew et al. concluded that the addition of Y can promote the $c + a$ slip, which accommodates the $c$-axis deformation and then alleviate the deformation anisotropy [15]. Furthermore, the addition of REs in magnesium alloys increases the stability of anti-oxide film on the surface [16], which would be helpful for the improvement of corrosion resistance.

## 2. Experimental

### 2.1. Preparation

Mg−REs−0.5Zr alloys were prepared in a steel crucible under a cover gas mixture of $CO_2$ and $SF_6$. After stirring at 730 °C for 0.5 h, the alloy was cast to the mould preheated at 500 °C. The filled mould was held at 670 °C for 30 min under the protective gas to let the heavy impurities settle to the bottom and the light impurities float up to the top of the ingots. Then the permanent mold direct chill casting was used to prepare the alloys [17]. The whole steel crucible with the melt was immerged into the continuous cooling water at a speed of 20 mm/s. As soon as the liquid level of inside melt is aligned with the height of outside water, the solidification process was finished. The weight of each obtained ingot is about 2 Kg. The detailed chemical compositions of the alloys analyzed by X-ray fluorescence spectrometer are shown in Table 1. The content of Y is a little lower than the nominal composition of 0.4%. The compositions of other REs are close to the designed compositions of 0.4%.

### 2.2. Microstructural observations

Microstructures were examined using optical microscope and scanning electron microscopy (SEM). The polished samples for optical observations were taken from the same locations. They were chemically etched in a solution of 8 g picric acid, 5 ml acetic acid, 10 ml distilled water and 100 ml ethanol. The optical microstructure was characterized using a light microscope (Reichert-Jung MeF3, Germany) with a polarization system. The specimens for SEM observations were electropolished after mechanical polishing. During electropolishing, no any water-containing agents were used. After polishing, the specimens were observed using SEM immediately.

Table 1
Chemical compositions of typical alloys (wt.%).

| Sample | Y % | Dy % | Gd % | Sm % | Zr % |
|---|---|---|---|---|---|
| Mg04YZr | 0.20 | | | | 0.029 |
| Mg04GdZr | | | 0.38 | | 0.203 |
| Mg04DyZr | | 0.38 | | | 0.209 |
| Mg04SmZr | | | | 0.44 | 0.180 |
| Mg04Y04GdZr | 0.28 | | 0.38 | | 0.154 |
| Mg04Y04DyZr | 0.27 | 0.36 | | | 0.193 |
| Mg04Y04SmZr | 0.21 | | | 0.46 | 0.210 |
| Mg04Gd04DyZr | | 0.45 | 0.38 | | 0.188 |
| Mg04Gd04SmZr | | | 0.38 | 0.46 | 0.209 |
| Mg04Dy04SmZr | | 0.36 | | 0.45 | 0.216 |
| Mg-04Gd04Dy04SmZr | | 0.34 | 0.38 | 0.45 | 0.217 |
| Mg−04Y04Gd04Dy04SmZr | | 0.35 | 0.38 | 0.44 | 0.209 |

### 2.3. Mechanical properties

The tensile and compressive tests were performed in accordance to DIN EN 1002 at room temperature using a Zwick 050 testing machine. For the tension tests, specimens with a gauge length of 25 mm and a diameter of 5 mm with threaded heads were used. The compressive samples had a length of 16 mm and a diameter of 11 mm.

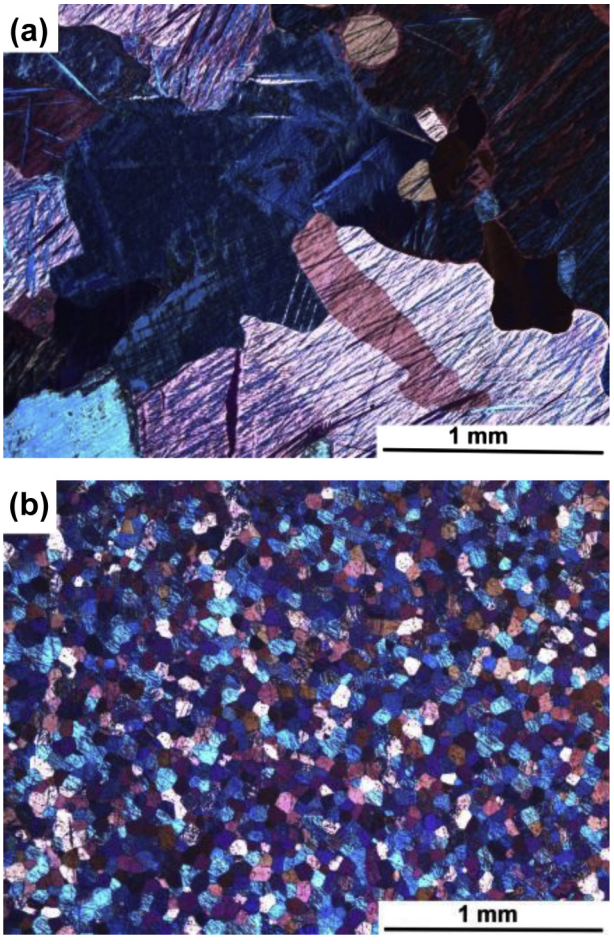


Fig. 1. Optical microstructures of Mg−0.4Y−0.4Gd−0.4Dy alloy, (a) without Zr and (b) with Zr.

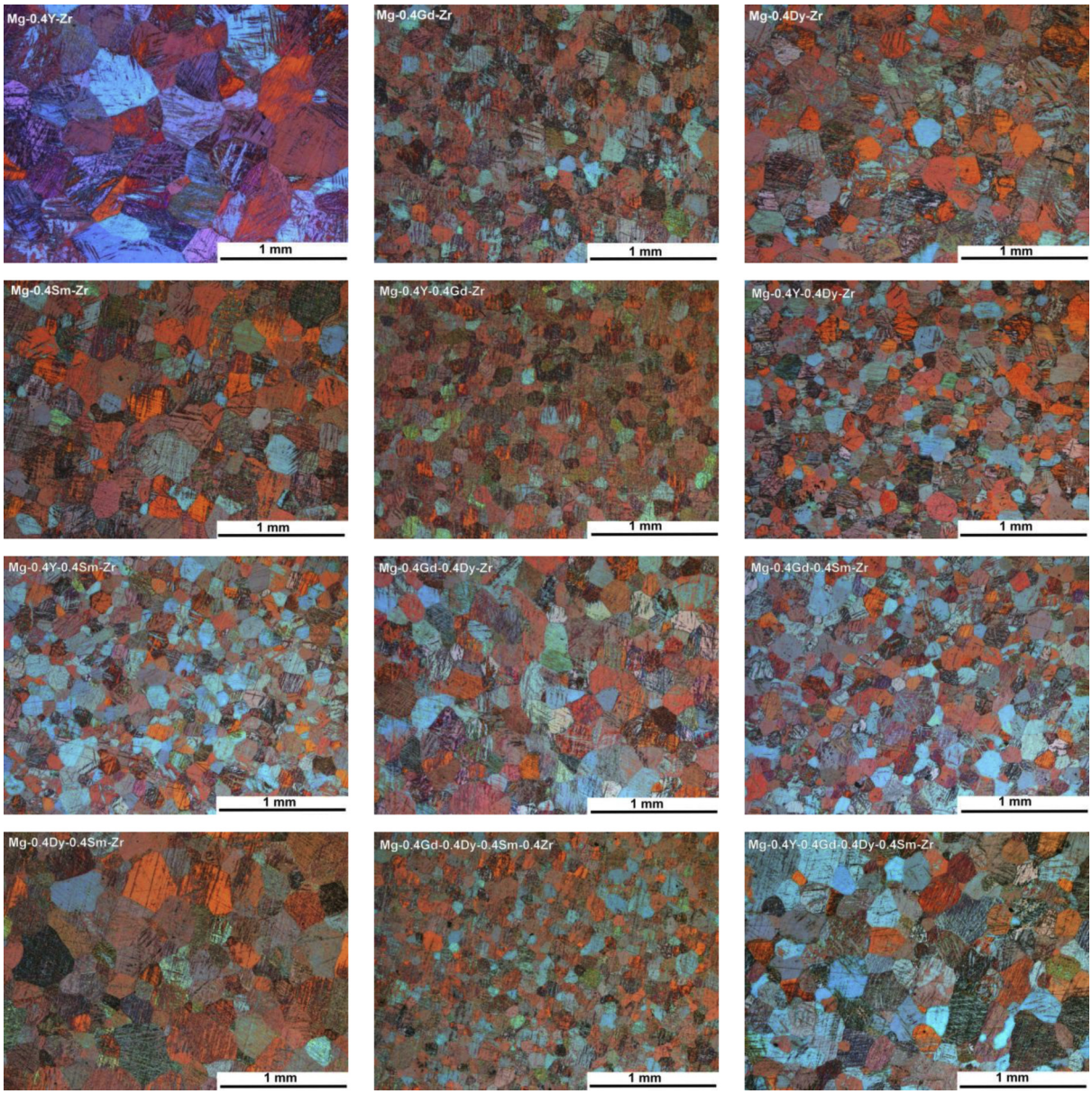


Fig. 2. Optical microstructures of Mg–RE alloys.

### 2.4. In situ texture analysis

Tensile specimen with a dimension of Ø6 × 35 mm was machined from the ingot. *In situ* experiment was performed at the neutron diffractometer STRESS-SPEC at FRM II (Heinz Maier-Leibnitz Zentrum, Germany) using a novel tensile rig [18]. The used wavelength was 1.748 Å from Ge (311) monochromator. The investigated gauge volume was $5 \times 5 \times 5\ mm^3$ controlled by a primary slit and a radial collimator in front of the detector. The texture measurement points were selected to some specific loads, i.e. under yield strength, strain hardening, hardening to platform transition, UTS (ultimate tensile stress) and broken. At each point the specimen was first pulled to a fixed load under a speed of 3.5 N/s; and then simultaneously fixed the position when reaching the load. Pole figure measurement was done using non-continuous phi rotation with 40 s per 5°.

### 2.5. Corrosion properties

The corrosion rate by immersing in 0.9 wt.% NaCl for 48 h was cross-checked by measuring the weight of the specimens before and after the corrosion test. The latter was done after cleaning and removal of all corrosion products in chromic acid ($180\ g\ l^{-1}$, 20 min immersion at room temperature). The average corrosion rate (Pi: $mm.y^{-1}$) of each specimen at the end of the tests was calculated by converting the total amount of material loss.

Electrochemical tests were carried out using a Gill AC potentiostat/frequency response analysis system to evaluate the corrosion behavior of the specimens. A typical three electrode cell, with a saturated Ag/AgCl (saturated with KCl) as reference electrode, a platinum mesh counter electrode and the investigated specimen as the working electrode ($0.5\ cm^2$ exposed area),

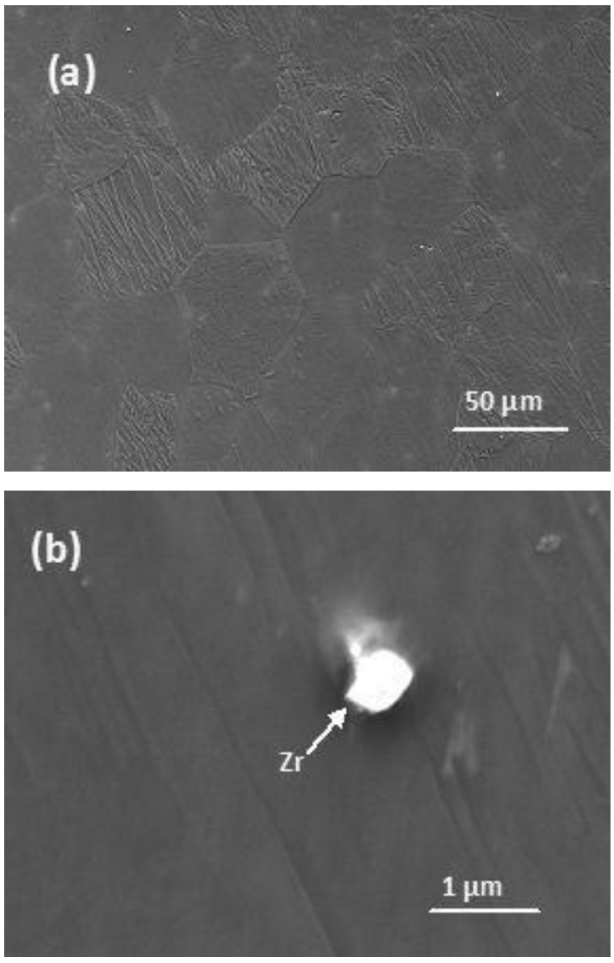


Fig. 3. (a) No second phases and (b) only the Zr particles in Mg–YGdDy–Zr alloys.

was used. All polarization tests were conducted in a 0.9 wt.% NaCl solution at a scan rate of 0.5 mV $s^{-1}$ after an exposure period of 30 min.

The polarization curves were used to estimate the corrosion current density ($i_{corr}$) at corrosion potential ($E_{corr}$) by Tafel extrapolation of the cathodic branch. The corrosion current density, $i_{corr}$ (mA $cm^{-2}$), can be related to the Pi (mm $y^{-1}$) using the following conversion equation [19].

$$P_i = 22.85 i_{corr} \quad (1)$$

According to the above conversion equation, the corrosion rates are calculated.

## 3. Results and discussion

### 3.1. Microstructural observations

The influence of Zr addition on the microstructure of Mg–RE alloy is shown in Fig. 1. The alloy without the addition of Zr has a very coarse grain. After the addition of Zr, the grain size is decreased to about 55 μm. The addition of Zr also changes the microstructure from the columnar to the equiaxed.

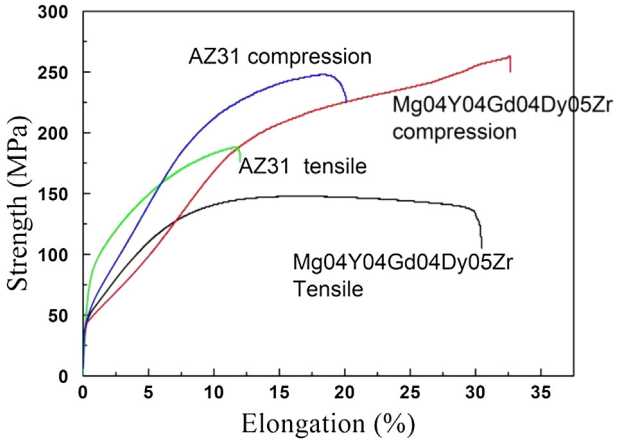


Fig. 4. Comparison of mechanical properties of Mg–RE alloy with the conventional AZ3 alloy.

Fig. 2 shows the optical microstructure of Mg–REs alloys. The equiaxed grains are dominated in all samples. However, the different alloys have a different grain size. Among all alloys, the grain size of Mg–0.4Y–Zr alloy is maximum. Chemical analysis indicated that the content of Zr in this alloy is very small with a value of 0.03 wt.% after casting, although 0.5 wt.% Zr was added to the melt before casting. The other alloys have a content of Zr about 0.2%. Thus, the large grain for Mg–0.4Y–Zr alloy is caused by the small content of Zr. The reason why this alloy has such a small of content of Zr is still unclear.

SEM observations demonstrate that there exists no other second phase except for the Zr particles (Fig. 3). The present designed Mg–REs alloys are therefore close to the single phase solid solution.

### 3.2. Mechanical properties

Fig. 4 compares the mechanical properties of the as-cast Mg–RE alloy with the as-cast conventional wrought AZ31 alloy. The tensile yield strength of Mg–RE alloy is close to that of AZ31 alloy, but the compressive yield strength much lower than that of AZ31 alloy. After Mg multi-microalloying with REs, the room temperature elongations for both compressive and tensile deformations are largely improved. They are much higher than that of AZ31 alloys. The tensile elongation of Mg–RE alloy reaches to about 30%, while AZ31 is only about 12%. In addition, it is very interesting that the difference between the tensile and compressive yield stresses is much smaller for Mg–RE alloy (2.4 MPa) than that (24.0 MPa) for AZ31 alloy. This means that the mechanical anisotropy of Mg–RE alloys is also alleviated by multi-microalloying with REs.

Table 2 lists the mechanical properties of Mg–REs alloys, including the tensile and compressive properties. Except for Mg–04Y–Zr alloy, the other Mg–REs alloys have a high elongation with more than 15%. The lowest ductility of Mg–04Y–Zr alloy is due to its coarse grain (Fig. 2). Compared with the alloys with the addition of single RE, the alloys with

Table 2
Mechanical properties at room temperature for Mg–RE alloys.

| Alloys | Tensile properties | | | Compressive properties | | |
|---|---|---|---|---|---|---|
| | YS (MPa) | UTS (MPa) | Strain (%) | YS (MPa) | UCS (MPa) | Strain (%) |
| Mg04YZr | 20.9 ± 1.0 | 119.3 ± 7.2 | 4.3 ± 2.5 | 25.6 ± 2.0 | 200.8 ± 16.6 | 15.6 ± 3.6 |
| Mg04GdZr | 52.2 ± 3.8 | 144.6 ± 1.7 | 22.1 ± 1.6 | 40.2 ± 1.1 | 231.3 ± 8.7 | 24.4 ± 1.5 |
| Mg04DyZr | 53.7 ± 3.0 | 140.7 ± 0.4 | 17.5 ± 0 | 32.5 ± 2.6 | 231.6 ± 16 | 22.7 ± 2.0 |
| Mg04SmZr | 51.6 ± 3.1 | 144.2 ± 6.5 | 17.0 ± 2.5 | 36.2 ± 1.6 | 237.1 ± 3.0 | 22.9 ± 2.6 |
| Mg04Y04GdZr | 51.7 ± 2.8 | 140.2 ± 0.6 | 27.7 ± 1.5 | 43.7 ± 2.7 | 242.4 ± 16.2 | 24.9 ± 0.2 |
| Mg04Y04DyZr | 48.9 ± 2.5 | 132.2 ± 1.5 | 29.3 ± 1.8 | 43.8 ± 1.6 | 247.7 ± 7.1 | 25.0 ± 0.3 |
| Mg04Y04SmZr | 55.7 ± 2.7 | 148.6 ± 2.9 | 27.0 ± 2.3 | 47.0 ± 5.7 | 260.8 ± 10.2 | 25.1 ± 0.2 |
| Mg04Gd04DyZr | 47.6 ± 2.7 | 143.7 ± 2.4 | 22.2 ± 2.2 | 38.1 ± 2.3 | 243.5 ± 4.7 | 25.6 ± 0.3 |
| Mg04Gd04SmZr | 51.7 ± 0.3 | 145.1 ± 3.6 | 26.4 ± 0.7 | 44.1 ± 0.8 | 247.5 ± 1.0 | 24.8 ± 1.0 |
| Mg04Dy04SmZr | 49.2 ± 2.1 | 148.4 ± 2.0 | 19.6 ± 2.5 | 38.2 ± 1.0 | 250.0 ± 9.3 | 24.7 ± 1.5 |
| Mg-04Gd04Dy04SmZr | 57.8 ± 1.9 | 140.8 ± 4.4 | 30.8 ± 0.6 | 50.9 ± 0.4 | 264.7 ± 2.0 | 26.5 ± 0.4 |
| Mg–04Y04Gd04Dy04SmZr | 49.6 ± 1.1 | 146.0 ± 1.3 | 17.4 ± 2.0 | 45.6 ± 1.6 | 249.4 ± 7.6 | 24.2 ± 2.0 |

*YS-Yield Stress; UTS –Ultimate Tensile Stress; UCS-Ultimate Compressive Strength.

multi-microalloying have a better tensile ductility. For the former, normally, the tensile elongation is about 17–22%, but for the latter, the tensile elongation is increased to more than 20%, even reaches to about 30% for Mg04Gd04Dy04Sm–Zr alloy. As shown in Table 2, the tensile elongation is also influenced by grain size. The alloys with a small grain have a higher tensile ductility. Unlike the tensile ductility, the tensile yield stress of Mg–REs alloys seems not to be affected by alloying with RE (single-alloying) or REs (multi-alloying). All Mg–REs alloys have a similar tensile yield stress with a value of about 50 MPa except for Mg–04Y–Zr alloy.

The compressive yield stress and tensile elongation are more sensitive to grain size. The alloys with a larger grain have a lower compressive yield stress and lower tensile elongation. Except for Mg–04Y–Zr alloy, the tensile yield stresses and compressive strain for other alloys are almost the same with a value of about 50 MPa and 25%, respectively. The difference between the tensile and compressive yield stress also depends on the grain size. The small grain can alleviate the mechanical anisotropy, which is in agreement with the previous results [20].

### 3.3. In situ texture analysis

Fig. 5(a) shows the texture measured point on the tensile curve and Fig. 5(b) plots the variation of maximum intensity of

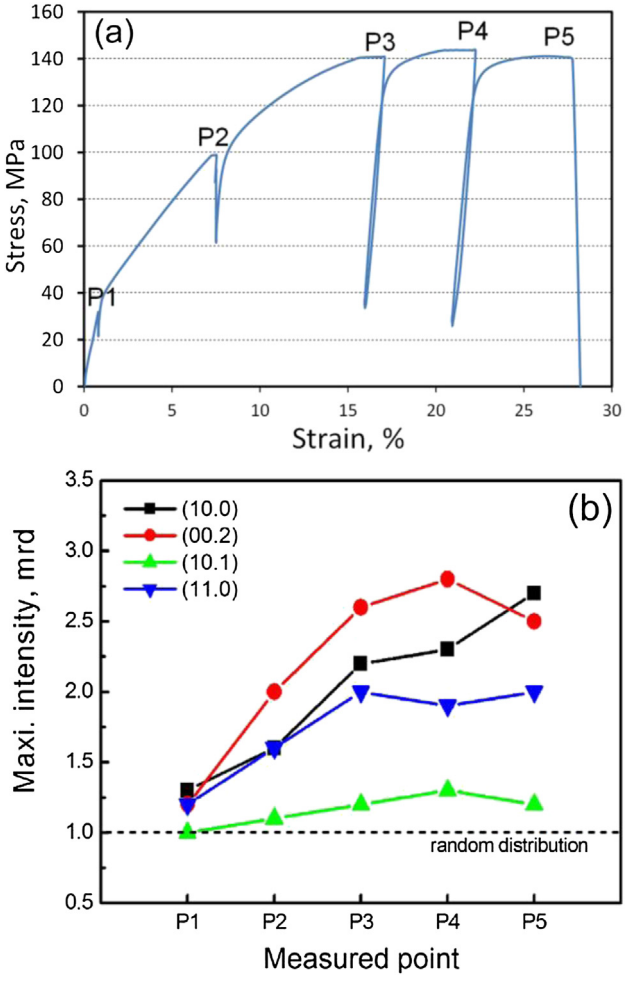


Fig. 5. (a) *In situ* tensile curve within the marked texture measured points; (b) maximum intensity variation of the four pole figures as indicated. Alloy: Mg–04Gd–Zr.

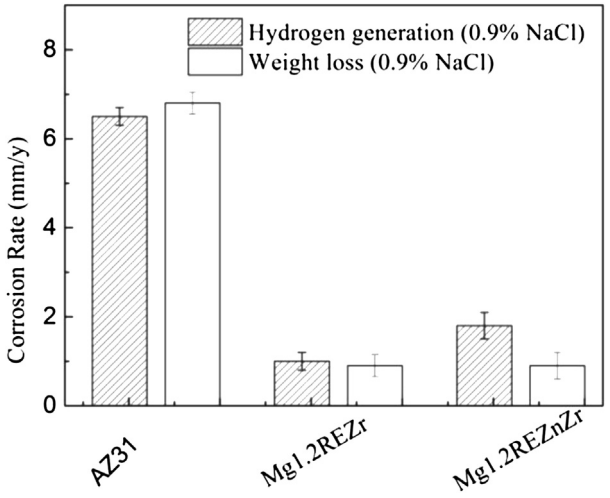


Fig. 6. Corrosion properties of Mg–RE alloys and AZ31 alloy in 0.9% NaCl solution.

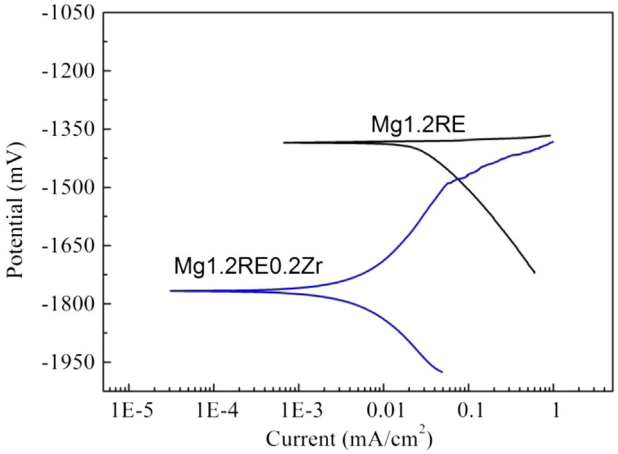


Fig. 7. Potentiodynamic polarization curves of Mg−RE alloys in 0.9 wt.% NaCl (after exposure for 0.5 h).

the pole figures (10.0), (00.2), (10.1) and (11.0), respectively. Point P1 before the yield strength shows a random orientation distribution. Fast increase of the intensity in (00.2) from P2 to P3 which are at the strong hardening stage indicates a predominated basal plane sliding. This <a> type basal plane sliding should also be accommodated by twinning or the <a> type prismatic plane {10.0} or {11.0} since their intensities show also a sharp increase. From P3 to P5 the (00.2) and (11.0) pole figure intensities remain nearly stable, while there is still a maximum intensity increase of (10.0) planes. Hence the <a> type prismatic plane sliding contributes a lot to this strain hardening platform which greatly increases the ductility of this Mg−RE alloy. Detailed descriptions together with the microstructures will be published later.

Compared with the commercial AZ31 the developed textures via *in situ* tensile deformation of this Mg−RE are very weaker which normally show half intensity of those of AZ31 alloy [21]. This indicates that the addition of RE could lead to a weakening of texture during deformation.

### 3.4. Corrosion properties

The corrosion results are shown in Fig. 6. The similar results are observed by evaluating hydrogen generation and weight loss. The corrosion rate of AZ31, Mg1.2RE0.2Zr and Mg1.2RE0.2Zn0.2Zr are 6.2 mm/y, 1.1 mm/y and 1.2 mm/y, respectively. Compared with the conventional AZ31 alloy, the corrosion resistance of Mg−RE alloys in NaCl solution is improved with 6 times. The improvement of corrosion resistance for Mg−RE alloys may be attributed to the following points: Firstly, the addition of rare earths elements can purify Mg matrix during casting and remove some harmful elements such as iron. It would be beneficial for the improvement of corrosion resistance [22,23]. Secondly, the stability of anti-oxide film can be improved by the addition of RE [24]. Thirdly, the single phase solid solution without precipitates would be highly helpful to alleviate the galvanic corrosion [25]. Due to the reduction of the $Mg_{17}La_2$-type intermetallic compound caused by quenching, the as-quenched Mg−Zn−La alloys showed a good corrosion resistance in the NaCl solution.

The corrosion behavior of the specimens evaluated by potentiodynamic polarization after exposing in 0.9 wt.% NaCl solutions for 0.5 h is presented in Fig. 7. Mg1.2RE alloy exhibits a high $i_{corr}$ ($-2.21 \pm 0.02 \times 10^{-1}$ mA/cm$^2$). After the addition of Zr, the $i_{corr}$ value is decreased to $-4.57 \pm 0.02 \times 10^{-2}$ mA/cm$^2$. More interestingly, the apparent breakdown platform of Mg1.2RE0.2Zr alloy is detected during corrosion. In contrast, the $E_{bd}$ has not been detected in Mg1.2RE alloy, which means that the unstable corrosion surface has been broken at the beginning of corrosion.

## 4. Conclusions

The as-cast magnesium alloys multi-microalloying with rare earths possess a quite high ductility with a tensile strain up to 25−30% at room temperature. The improved elongation is closely associated with the additions of REs, small grains and elimination of large second precipitates. Compared with AZ31 alloy, these alloys have a lower mechanical anisotropy. The preliminary *in situ* neutron diffraction investigations on the tensile deformation of these alloys indicate that the multi-microalloying with rare earths seems to be beneficial for the activation of non-basal systems. The deformation becomes more homogeneous and the resultant textures after deformation are weakened. These Mg−REs−Zr alloys exhibit a much better corrosion resistance than AZ31 alloy in NaCl solution.

## Acknowledgments

The authors would like to thank Mr. Willi Punessen and Mr. Günter Meister for their technical assistances.

## References

[1] K.U. Kainer, Magnesium Alloys and Technology, Wiley-VCH GmbH, Weinheim, Germany, 2003.
[2] H.E. Friedrich, B.L. Mordike, Magnesium Technology Metallurgy, Design Data, Applications, Springer-Verlag, Berlin Heidelberg, 2006.
[3] B. Bhattacharya, M. Niewczas, Philos. Mag. 91 (2011) 2227−2247.
[4] J. Koike, Metall. Mater. Trans. A 36A (2005) 1689−1696.
[5] G.L. Song, A. Atrens, Adv. Eng. Mater. 1 (1999) 11−33.
[6] G.L. Song, A. Atrens, Adv. Eng. Mater. 5 (2003) 837−858.
[7] G.L. Song, Corrosion of Magnesium Alloys, Woodhead Pub Limited, 2011.
[8] Q. Peng, Y. Huang, K.U. Kainer, N. Hort, Adv. Eng. Mater. 14 (2012) 178−184.
[9] Q. Peng, Y. Tian, Y. Huang, N. Hort, Mater. Lett. 83 (2012) 209−212.
[10] E.F. Emley, Magnesium Technology, Pergamon Press, London, 1966.
[11] N. Stanford, D. Atwell, A. Beer, C. Davies, M.R. Barnett, Scr. Mater. 59 (2008) 772−775.
[12] N. Stanford, M. Barnett, Scr. Mater. 58 (2008) 179−182.
[13] J. Bohlen, M.R. Nürnberg, J.W. Senn, D. Letzig, S.R. Agnew, Acta Mater. 55 (2007) 2101−2112.
[14] M.R. Barnett, A. Beer, D. Atwell, C.H.J. Davies, T. Abbott, in: S.R. Agnew, M.R. Neelameggham, E.A. Nyberg, W.H. Sillekens (Eds.), Magnesium Technology 2010, The Minerals, Metals & Materials Society (TMS), Seattle, Washington, USA, 2010, pp. 353−357.
[15] S.R. Agnew, M.H. Yoo, C.N. Tomé, Acta Mater. 49 (2001) 4277−4289.
[16] J. Zhang, X. Niu, X. Qiu, K. Liu, C. Nan, D. Tang, J. Meng, J. Alloys Compd. 471 (2009) 322−330.

[17] Q. Peng, Y. Huang, L. Zhou, N. Hort, K.U. Kainer, Biomaterials 31 (2010) 398−403.
[18] M. Hoelzel, W.M. Gan, M. Hofmann, C. Randau, G. Seidl, P. Juettner, W.W. Schmahl, Nucl. Instrum. Methods Phys. Res. Sect. A 711 (2013) 101−105.
[19] M.-C. Zhao, M. Liu, G.-L. Song, A. Atrens, Corros. Sci. 50 (2008) 3168−3178.
[20] J. Bohlen, P. Dobron, E.M. Garcia, F. Chmelik, P. Lukac, D. Letzig, K.U. Kainer, Adv. Eng. Mater. 8 (2006) 422−427.
[21] S.B. Yi, C.H.J. Davies, H.G. Brokmeier, R.E. Bolmaro, K.U. Kainer, J. Homeyer, Acta Mater. 54 (2006) 549−562.
[22] J.E. Hillis, Light Met. Age 41 (1983) 25−29.
[23] O. Holta, H. Westengen, D. Albright, in: G. Lorimer (Ed.), International Congress & Exposition, SAE, Detroit, Michigan, United States, 1994, pp. 1−5.
[24] W. Liu, F. Cao, L. Chang, Z. Zhang, J. Zhang, Corros. Sci. 51 (2009) 1334−1343.
[25] G. Song, Adv. Eng. Mater. 7 (2005) 563−586.